Transit currents in a one-dimensional polymer single crystal

1992 J. Phys.: Condens. Matter 4 2517

(http://iopscience.iop.org/0953-8984/4/10/015)

J. Phys.: Condens. Matter 4 (1992) 2517–2532. Printed in the UK

Transit currents in a one-dimensional polymer single crystal

N E Fisher† and D J Willock‡

† Department of Physics, King's College London, Strand, London WC2R 2LS, UK
‡ Chemistry Department, University College London, Christopher Ingold Laboratories, 20 Gordon Street, London WC1H 0AJ, UK

Received 14 August 1991

Abstract. Time-of-flight experiments are performed on the one-dimensional semiconductor single-crystal PDATS using localized carrier generation on the (100) face. We present new results and conclusions based on these techniques. Carrier velocities are found to be field dependent, acoustic and trap limited with an inter-trap separation of 15 μm or less. A simple model is proposed to explain this field dependence and is based on the premise that the intrinsic motion of the negative carriers is that of a solitary wave acoustic polaron as advanced by Wilson, but whose observed motion is dominated by shallow, field-dependent traps with trap release times at room temperature that are inversely proportional to field. Time-of-flight signals for holes were not observed and it is concluded therefore that the electrons are the dominant current carriers. Also, the length dependence of the transit times is found to be linear, suggesting that electron propagation is Gaussian. Finally, the effects of electrode geometry and charge density on field are considered.

1. Introduction

1.1. PDATS

PDATS (the polymer bis(*p*-toluene sulphonate) ester of 2,4-hexadiyne-1,6-diol) is easily produced as millimetre-sized single crystals in which the polymer backbone direction is well defined and common to all chains in the sample [1]. Because the chain separation is large (0.7 nm) compared with the repeat unit distance on a chain (0.45 nm) [2], each may be considered as an independent, quasi-one-dimensional semiconductor. Dark-conductivity measurements along and perpendicular to the chains by Siddiqui and Wilson show an anisotropy of over 1000 reflecting this one-dimensional nature [3]. Experiments on PDATS may, then, offer an insight into one-dimensional carrier motion.

Work by Batchelder *et al* [4] has shown that crystal quality can be degraded by the presence of oxygen. The crystals used here were therefore grown with care taken to prevent oxygen contamination [5]. The effect of oxygen on carrier motion has also been investigated by the authors and will be the subject of a future publication.

1.2. Transit currents

A useful technique for measuring the carrier mobility in any material is the time-of-flight method due to Kepler and LeBlanc [6, 7]. Figure 1 shows the usual experimental set-up for observing these transit signals. A sample of length L is provided with

0953-8984/92/102517+16$04.50

two electrodes (one semi-transparent) in a sandwich arrangement. The carriers are generated by a light pulse incident on the semi-transparent electrode and absorbed in a skin depth that is much less than L. The sheet of carriers created is then transported across the sample under the action of the applied field $F = V/L$. As they drift, they induce a time-dependent current $I(t)$ in the external circuit, which is observed. When the carriers reach the other electrode and discharge, $I(t)$ drops suddenly, and it is the time of this transition region that is taken as the transit time. For the ideal case where the carrier sheet undergoes no dispersion, the transit current profile is shown in figure 2(a). However, with dispersion present, the transition region no longer shows a sharp drop, but instead broadens into a tail, with the width of the tail a measure of the degree of this dispersion. This case is shown in figure 2(b). Taking the position of the shoulder as indicating the transit time, an unambiguous drift velocity and mobility for the faster carriers may therefore be determined from the relations

$$v_d = L/t_\tau \tag{1}$$

$$\mu = v_d/F \tag{2}$$

respectively. By reversing the polarity of the applied field, the drift and carrier mobility for the other sign of carriers may be deduced.

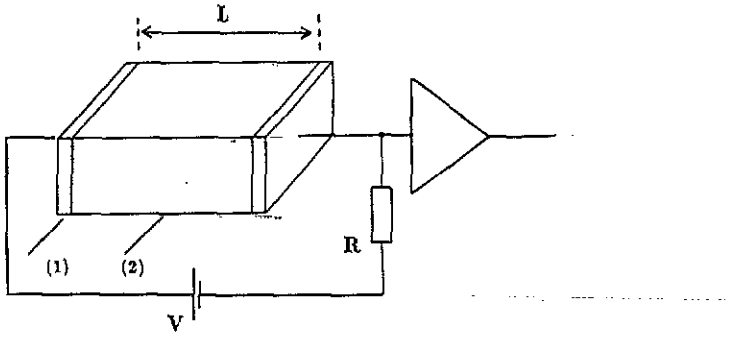

Figure 1. Layout for a conventional Kepler LeBlanc transient photoconductivity measurement. (1) Semi-transparent electrode. (2) Sample of length L.

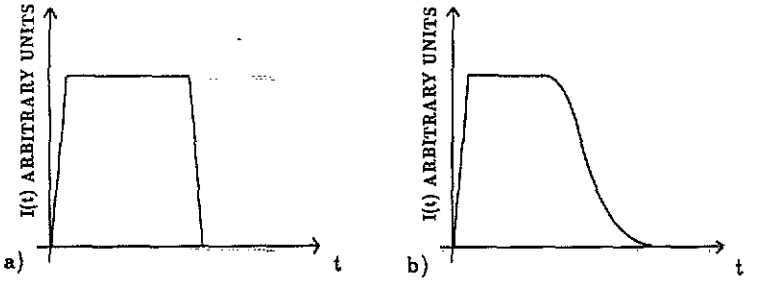

Figure 2. (a) Transit current profile with no dispersion present. (b) Transit current profile with dispersion present.

The mode of propagation of a carrier packet can be broadly classed into two catagories:

(i) Gaussian propagation. Here, the carrier packet broadens symmetrically about its mean position as it traverses the sample length. Gaussian statistics predict a linear dependence of t_τ on L, and such propagation has been observed in crystals such as anthracene [8].

(ii) Non-Gaussian or dispersive propagation. In this case, the carrier packet undergoes a significant broadening as it drifts through the sample. Owing to the wide distribution of statistical event times, which extends into the time range characteristic of the experiment (t_τ), Gaussian statistics can now no longer be applied. Such broadening is usually associated with considerable disorder in the sample, and has been observed in, for example, a-Ase_2Se_3 [9]. The most successful statistical theory for describing this transport is that due to Montroll and Scher [10]. Here, a non-linear length dependence of t_τ on L is predicted and such behaviour has been observed [11]. An analogous model for dispersive transport in one-dimensional systems has been put forward by Movaghar *et al* [12]. Again, a non-linear length dependence of t_τ on L is predicted.

These differences in length dependence between the two modes of carrier propagation will be used to deduce the mode of carrier transport in the PDATS samples used here.

2. Experimental arrangement

Experiments using a conventional Kepler LeBlanc configuration have been performed on PDATS by Bassler and Reimer [13] where sample lengths were about 100 μm. Time-of-flight signals were observed but of unknown sign. However, the morphology of the crystals leads to the polymer chains being orientated at 22° to the applied field. This means that the carriers may not be confined to single chains during transport, and that inter-chain motion may be the limiting factor on the carrier mobility.

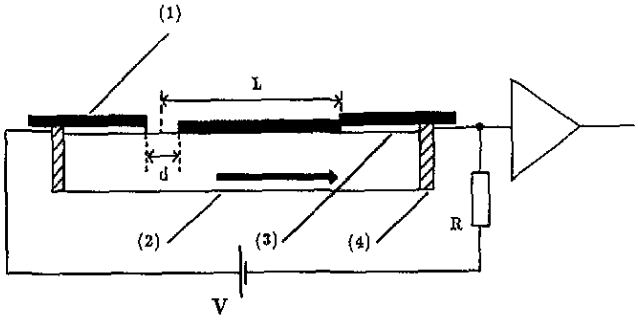

Figure 3. Experimental arrangement for a transit current experiment on the (100) face in PDATS. (1) Opaque optical mask with slit width d. (2) PDATS crystal. (3) Evaporated Ag electrodes. (4) Silver-paste.

A simpler and perhaps more straightforward method for observing transit signals in PDATS is shown in figure 3 and was first reported in [14]. In this type of surface arrangement, the slit is positioned on the (100) face, perpendicular to the chains and

next to one electrode. Following a 10 ns laser pulse of photon energy 3.68 eV, a sheet of carriers is generated in a skin depth of 0.5 μm at the slit. Carriers of one sign, depending on the polarity of V, traverse the sample, to induce a transit signal, while those of the other sign discharge almost immediately at its nearest electrode. To observe the transit signals induced by carriers of the opposite sign, the polarity of the applied voltage is reversed. Since the skin depth is small compared with the inter-electrode distances, the field sampled by the carriers is approximately uniform. The field at the electrodes will be discussed shortly. The drift velocity and carrier mobility can thus be determined from the relations (1) and (2) respectively where, here, L is the average distance traversed by the carrier packet and is taken to be

$$L = D - d/2 \tag{3}$$

where D is the inter-electrode spacing and d is the slit width. The applied field is now given by $F = V/D$.

These transit signals are observed using a fast oscilloscope (Tektronix 7A26) and amplifier system with an overall response time of 10 ns. All experiments were performed with the samples under a vacuum of 10^{-6} Torr.

3. Results

3.1. Profiles

The following results, unless otherwise specified, were obtained using a sample length (D) of 300 μm and a slit width (d) of 60 μm. Figure 4 shows the induced current profiles for negative V (upper trace) and for positive V (lower trace). Both traces exhibit an initial fast response followed by a decay. We consider this decay to be due to the deep trapping (where trap release times are greater than t_r) of a proportion of the sheet of carriers as they traverse the sample length. As can be seen, a transition shoulder (due to the surviving faster carriers) is only observed for the electrons. This asymmetry of current profiles, with respect to the polarity of V, was observed at all the applied fields used here (ranging from 1×10^5 to 1×10^7 V m^{-1}). We therefore deduce that the negative carriers are the dominant current carriers, and that the featureless current profiles observed when V is positive may, in fact be dominated by the drift and discharge of the electrons at their nearest electrode.

The typical field dependence of the profiles for the negative carriers is shown in figure 5. Not only is the transition region field dependent but also these signals exhibit more dispersive profiles as the field is decreased. In fact, at fields of less than 5×10^5 V m^{-1}, the transition region is no longer visible and only a featureless decay is seen. At the highest fields a small peak is observed in the transition region. To explain this, we have to consider the non-uniformity of the field close to one electrode. Near its edge we would expect the field to be larger than elsewhere. This may be investigated and quantified by observing the difference in the initial field-dependent peak photocurrent I_p induced by a sheet of carriers created close to one electrode and a sheet created at $D/2$ for the same applied V, and then using the simple relation

$$\frac{I_p(\text{generated near electrode})}{I_p(\text{generated at } D/2)} = \left(\frac{F(\text{near electrode})}{F(\text{at } D/2)}\right)^x \tag{4}$$

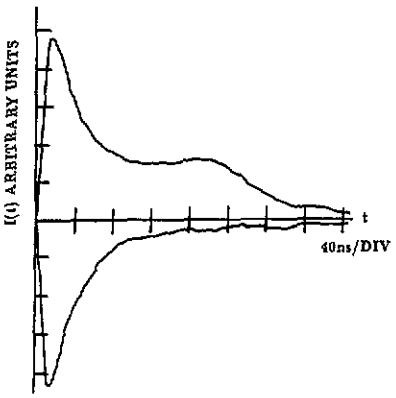

Figure 4. Current profiles for V negative (upper trace) and V positive (lower trace). The incident laser intensity is 1×10^5 W m^{-2} and F is 2.47×10^6 V m^{-1}.

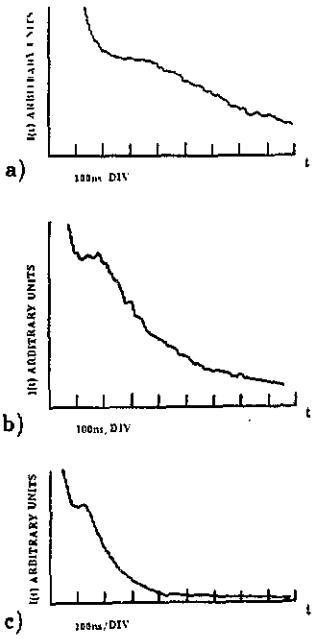

Figure 5. Field dependence of the current profiles for the negative carriers using incident laser intensity 1×10^6 W m^{-2}. (a) F is 8.17×10^5 V m^{-1}. (b) F is 1.33×10^6 V m^{-1}. (c) F is 3.33×10^6 V m^{-1}.

to find the ratio of the local fields. Here X is the exponent in the superlinear field relation between I_p and F usually found for PDATS at higher fields [15, 16]. Using a sample of length 520 μm and the slit to localize carrier generation, figure 6 shows the current profiles for the slit positioned (a) close to the left electrode, (b) near the sample centre and (c) close to the right electrode. It can be seen that illumination adjacent to either electrode results in a peak photocurrent about six times larger than for the slit positioned at $D/2$. With X, using this arrangement, found to be 1.5, the ratio of local fields is about three. However, from the general result that

$$I(t) = (q/V)\ \mathrm{d}V(x)/\mathrm{d}t \tag{5}$$

where q is the carrier charge and x is the carrier position, this factor of three must be an upper bound since the potential change $\mathrm{d}V(x)$ through which the carriers drift is greatest at the electrode.

In the transit experiment then, a sheet of carriers approaching the absorbing electrode will induce a larger current than a sheet at $D/2$ due to the larger field. This will lead to the observed peaks in the transition region. However, dispersion of the sheet at low fields will tend to wash out this peak leaving a residual shoulder. In all our experiments and at all fields, this peak is always very small compared with the overall current profile. This suggests to us, along with our upper-bound estimate for the ratio of local fields, that this non-uniformity across the sample surface is not excessive.

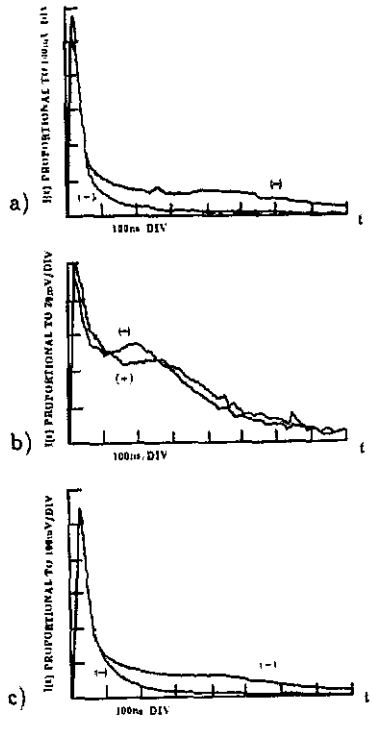

Figure 6. Current profiles when illuminating (a) at the left electrode, (b) near the centre, (c) at the right electrode. (+) left electrode positive. (−) left electrode negative. The laser intensity is 1×10^5 W m^{-2}. F is 1.0×10^6 V m^{-1}.

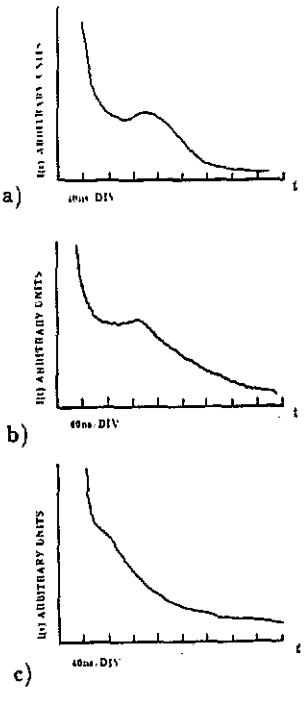

Figure 7. Intensity dependence of the current profiles for the negative carriers at $F = 3.33 \times 10^6$ V m^{-1}. The laser intensity is (a) 1×10^5 W m^{-2}, (b) 1×10^6 W m^{-2}, (c) 1×10^8 W m^{-2}.

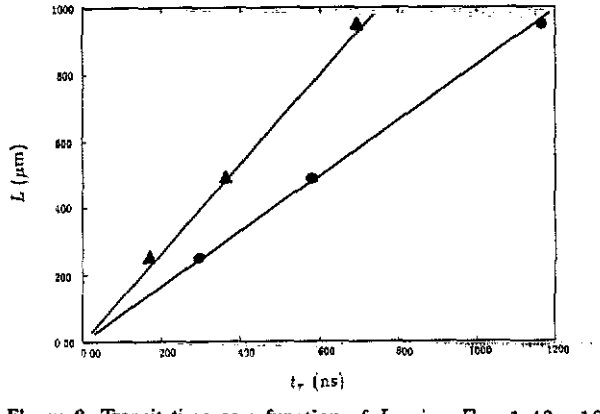

Figure 8. Transit time as a function of L using $F = 1.43 \times 10^6$ V m^{-1} (triangles) and $F = 7.14 \times 10^5$ V m^{-1} (circles) with laser intensity 1×10^5 W m^{-2}.

Figure 7 illustrates the intensity dependence of the transit profiles. More dispersive profiles and shorter transit times are observed as the intensity is increased.

We consider this to be a consequence of space charge effects when the condition $Q \ll CV$, where Q is the net charge present in the sample and C is the sample capacitance, is not satisfied. That is, with a large enough Q, for a given V, the internal applied field is appreciably disturbed by the presence of the charge. One can show qualitatively how the field is affected, by considering a parallel plate system with a negative V applied to one plate, zero potential applied to the other, and a strip of negative charge between the two. Using Poisson's equation to find the new disturbed field distribution between the plates, it is straightforward to show that with a large enough Q, the leading edge of the carrier sheet experiences a raising of the applied field while its back edge is subjected to a lowering. This raising of the field would result in a shorter observed transit time, because the carriers at the front edge drift faster, but also accompanied by a more dispersive transit profile because those at the back drift more slowly. These characteristics are observed in our experiments as Q is increased by raising the laser intensity, while keeping V constant. Further, estimates for Q and C in our experiments show that at low light intensities (for all the values of V used here), the condition $Q \ll CV$ is satisfied, but at the higher intensities it is not [17]. We conclude, therefore, that space charge effects are responsible for these changes in current profile. Similar effects in Kepler LeBlanc transit experiments have been well documented and indeed quantified by, for example, Many *et al* [18, 19] and also Schwartz and Hornig [20]. Therefore, for the following results, care was taken to ensure that the condition $Q \ll CV$ is well satisfied.

3.2. Length dependence

In this set of experiments, three samples cut from the same crystals are used. Here, D is 980, 520, and 280 μm. Figure 8 shows the transit time as a function of L at two different applied fields. Figure 9 shows the transit profiles for each of the sample lengths obtained at one of the fields. This, we shall refer to later. It is clear that at both the fields, t_τ scales linearly with L. This linearity with transit length is also evident from the data of figure 6.

As mentioned in section 1.2 non-Gaussian dispersive transport would give a non-linear length dependence and, as shown by Movaghar *et al* [12] for one-dimensional systems, follows the relation

$$t_\tau \propto FL^{1/(1-\alpha)} \tag{6}$$

where α is a disorder parameter and less than unity. Specifically for PDATS α has been measured to be 0.85 [12], implying that

$$t_\tau \propto FL^{6.66} \tag{7}$$

Clearly therefore, the mode of propagation of the carrier packet in the experiments presented here is Gaussian.

3.3. Field dependence of drift velocity

Figure 10 shows the field dependence of the negative-carrier drift velocity obtained using equation (1) for several different samples. Inspection of these results shows that:

(i) there is only small sample-to-sample variation;

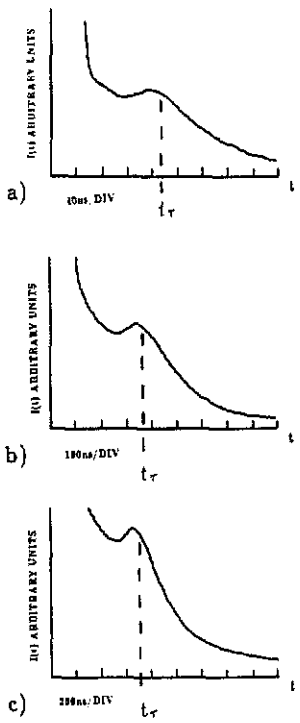

Figure 9. Length dependence of current profiles. (a) L is 250 μm. (b) L is 490 μm. (c) L is 950 μm. F is 1.43×10^6 V m^{-1}.

(ii) at low fields the data tend to a linear dependence of drift velocity on field. This linearity gives a negative-carrier mobility of 8.0×10^{-4} m^2 V^{-1} s^{-1};

(iii) at high fields the velocity tends towards saturation with field. The magnitude of this saturated velocity is comparable to the speed of sound in the chain direction (about 5000 m s^{-1} [21]).

This saturation (item (iii)) is a feature of the mode of carrier transport in one-dimensional systems as proposed by Wilson [22]. The experimental evidence pertaining to this, as found by Donovan and Wilson, will be discussed later. Here, current carriers are formed from the interaction of electrons (or holes) and the acoustic phonon field. These hybrid states are termed solitary wave acoustic polarons (SWAPs). Another property of the SWAP, according to Wilson is that the carrier velocity is saturated at all observable fields. Since our results suggest field saturation only at the highest applied fields, the mode of carrier transport cannot simply be that of the SWAP travelling unimpeded across the sample length. Rather, the intrinsic motion along a chain may be that of the SWAP, but the observed motion is dominated by field-dependent trapping (and/or barrier crossing) events. We now propose a simple model, based on the SWAP concept and the presence of shallow (where the trap release times are less than t_τ) Coulomb trapping. We concentrate on traps as opposed to barriers, since temperature dependence experiments on transit signals show activated behaviour. These experiments will be the subject of a future publication.

Consider figure 11. Following generation, the SWAP drifts along the chain at its intrinsic velocity, v_0, until it encounters a trap into which it falls. After a time τ_b it

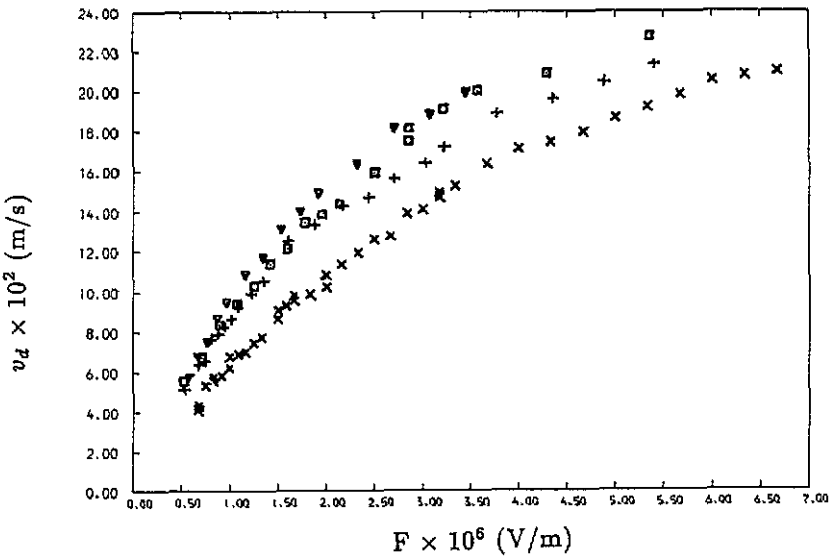

Figure 10. Field dependence of the drift velocity for various samples. Triangle: L is 490 μm. Square: L is 250 μm. Cross-hair: L is 340 μm. Diamond cross-hair: L is 270 μm.

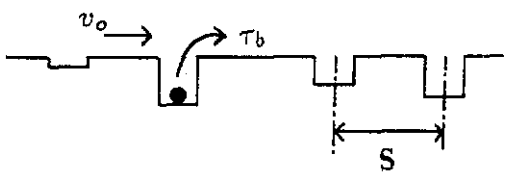

Figure 11. Representation of trap-limited transport of a carrier along a chain.

is released, thereafter to continue its motion along the chain until it encounters the next trap. If the average distance the carrier has to traverse is L, and if no traps are present, then the time it takes to cover this distance is $L/v_0 = t_0$. If there are N traps present within L, then the observed transit time is

$$t_\tau = t_0 + N\tau_b \tag{8}$$

where $N\tau_b$ is the total delay time due to traps. In general, the probability per unit time of trap escape is

$$1/\tau_b = \langle t(a)\phi(a)\rangle \tag{9}$$

where $t(a)$ is the probability in unit time that a trapped carrier, due to a thermal process, ionizes and acquires thermal kinetic energies at a distance a from the trap, and $\phi(a)$ is then the probability that the carrier avoids returning to the trap. The brackets $\langle\cdots\rangle$ denote an average over a. Wilson shows [23] that for charged traps the trap release time is given by

$$\tau_b = (A/F)\exp(\Delta E/kT) \tag{10}$$

where A is a temperature- and field-independent constant and ΔE is the activation energy of the trap. Substituting this into (8), and dividing into L, to gain an expression for drift velocity, gives

$$v_d = \frac{1}{[1/v_0 + (C/F)\exp(\Delta E/kT)]} \qquad (11)$$

where $C = NA/L$, and N, in the context of experiment, is the number of traps of average depth ΔE sampled by the faster carriers traversing the distance L.

Using the data of figure 10, the validity of equation (11) can be tested by plotting $1/v_d$ against $1/F$. These should yield linear plots with an intercept on the ordinate axis giving $1/v_0$, i.e. with near-infinite field the trap release times tend towards zero. Figure 12 shows these; over the limited field range possible, these plots do show reasonable linearity. Extrapolation of them yields an intrinsic drift velocity of between 3000–4000 m s^{-1} in accord with the SWAP model.

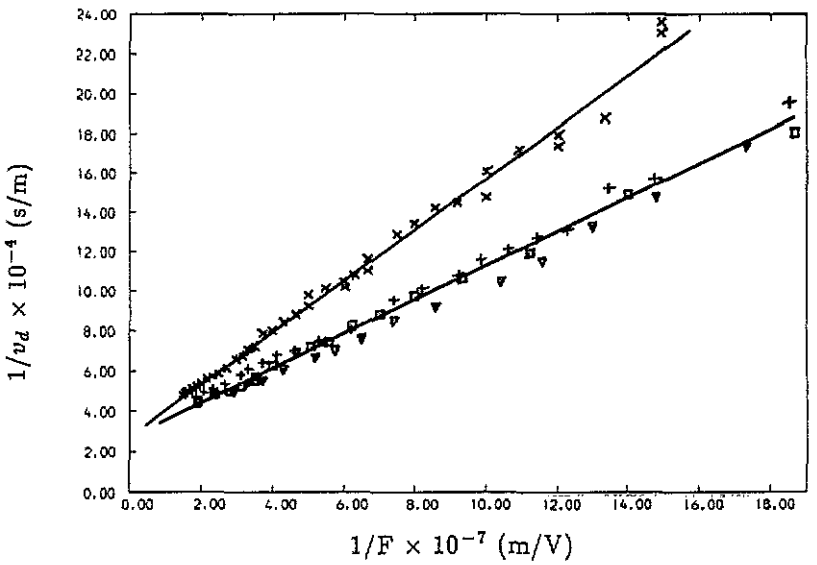

Figure 12. Plots of data from figure 10 following equation (11).

In the light of this model we now return to the observation that profiles become more dispersive as the field is reduced. For the Coulomb traps, the reduction in field will lead to an increase in the trap release times. This implies a greater range of release times, giving rise to the observed increase in dispersion. As the field is further reduced, the smearing of the transit shoulder becomes so marked that it eventually resembles a featureless decay with no discernible transit shoulder. This we consider analogous to the temperature dependence results reported by Pfister and Scher [11] in their transit experiments on a-Se. Here, a transition from non-Gaussian propagation at low temperatures to Gaussian propagation at higher temperatures is observed. Marshall [24] accounts for this by suggesting that if multiple trapping that is strongly temperature dependent takes place, then raising the temperature will reduce the trap release times sufficiently that Gaussian dispersion may be expected. At present, we have no real evidence to suggest that the Gaussian propagation we observe at the

higher applied fields changes to non-Gaussian propagation at low fields. However, we merely suggest that this may be the case, in view of the very dispersive transit profiles observed at the low fields.

3.4. The inter-trap separation

Equation (11), used to describe carrier propagation in the transit experiments, is based on the idea of distinguishing between the intrinsic free-chain motion, and the observed trap-limited motion. To estimate the range of this free motion, a knowledge of the mean inter-trap separation s is required (see figure 11). A value for the trap density occurs in the constant C of equation (11). However, it is not possible, without making further assumptions, to calculate the trap density directly since C is a convolution of this quantity and the individual trap release times. What can be said, however, is that for trap-limited transport to be observed, trapping centres must be present in the transit length L, and so this provides an upper limit for the inter-trap separation. In view of this we performed a time-of-flight experiment, using a slit width of 15 μm, on a sample with an inter-electrode gap of 60 μm. The field dependence for this sample showed the same behaviour as that for the longer samples. We conclude therefore that the inter-trap separation must be 52 μm or less. Further, when the polarity is reversed, no hole transit is observed (as expected), but the profile shape is found to be field dependent with, as can be seen from figure 13, the featureless decay narrowing as the field is increased. We consider this to be a result of the discharge of electrons at their nearest electrode. That is, as the field is increased the narrowing of the decay can be explained by the increase of electron velocity with field due to faster trap release times. This reasoning is similar to that in the sweep-out experiments of Heeger *et al* [25, 26]. Here, the whole of the (100) face is illuminated (uniform illumination) by a fast (picoseconds) light pulse and the currents, induced on surface electrodes, observed. These currents, following an initial peak , fall quickly to zero reflecting the rapid discharge of carriers at the electrodes. The time at which the current reaches zero is defined as the transit time t_τ. Thus, the carrier drift velocity is

$$v_d = D/2t_\tau \tag{12}$$

where D is the inter-electrode spacing and the term $D/2$ is the average distance traversed by the carriers. For sweep-out to occur, the sample lengths must be of the order of or shorter than the average distance traversed by the carriers before deep trapping or recombination events, and it seems that in order to achieve sweep-outs using PDATS the sample lengths must be of the order of 10–25 μm. These sweep-outs, as with our observations, exhibit a narrowing of the current profile with increasing field and it is this similarity of profile change with field that lead us to conclude that the sweep-out experiments and our slit experiment using a positive polarity of voltage are qualitatively similar because of the relative immobility of the holes. More detailed comparisons between our results and those of Heeger *et al* will be made in the next section.

4. Comparison with other work

The measurement of carrier mobility along the chain direction in PDATS has been approached in several different ways. Probably the most controversial are the measurements of Donovan and Wilson [15] using uniform illumination techniques. Here,

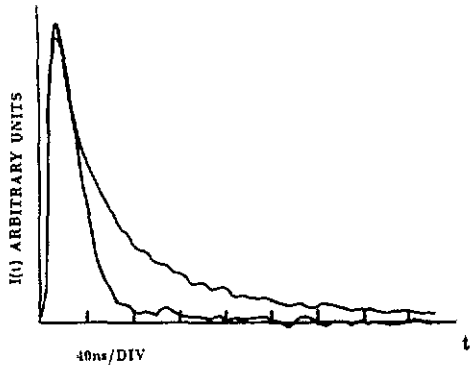

Figure 13. Field dependence of current profiles for positive V. Current heights are kept the same. Narrow profile: laser intensity is 1×10^5 W m^{-2}, F is 2.2×10^6 V m^{-1}. Broader profile: laser intensity is 3.3×10^6 W m^{-2}, F is 2.2×10^5 V m^{-1}.

their analysis is based on expressions for the peak photocurrent I_p, and the total charge transferred to the electrodes Q_m, following a single laser pulse. These expressions are given by

$$I_p = Qv_d/D \qquad \text{for } T_L < \tau \tag{13}$$

$$Q_m = Qs_r/D \tag{14}$$

where Q is the total charge generated by the pulse, T_L is the duration of the light pulse, D is the inter-electrode gap, v_d is the carrier velocity, τ is the mean free-carrier trap time and s_r is the mean distance travelled by a carrier before bulk recombination.

According to a set of experiments by Donovan and Wilson (see, e.g., [27]), all the charge generated eventually reaches the electrodes, i.e. bulk recombination is negligible, thus $s_r = D$ and so

$$Q_m = Q \tag{15}$$

Using equations (13) and (14) then, Donovan and Wilson obtain

$$I_p/Q_m = v_d/D \qquad \text{for } T_L < \tau. \tag{16}$$

They deduce from this an acoustic drift velocity of about 2000 m s^{-1} that is independent of field down to the lowest fields at which their measurements prove possible. In addition, their analysis of photocurrent decays following a 10 ns laser pulse indicates, in their opinion, a trap separation of the order of 1 mm [28]. Thus, Donovan and Wilson conclude that they are observing the intrinsic trap-free drift of the SWAP for macroscopic distances along the polymer chains. Further, because this drift velocity is saturated even at the lowest field, this can give rise, in their opinion, to an ultra-high low-field mobility, in excess of 20 m^2 V^{-1} s^{-1}.

On the other hand Blum and Bassler [29], using similar techniques, find a drift velocity that is weakly field dependent for fields less than 5×10^5 V m^{-1}, and starts

approaching a linear relation for fields greater than 2×10^6 V m^{-1}. In their analysis of current decays following a 10 ns laser pulse, they conclude that the drift velocity is defect controlled down to the smallest timescales experimentally accessible, and that it is this presence of numerous defects that is responsible for the field dependence of the drift velocity. These contradictory conclusions obtained using similar experimental techniques seem to show an openness to interpretation of the data (for instance, the analysis of current decays). That being said though, we consider the conclusions of Blum and Bassler, as far as charge transport is concerned, much in accord with our own observations.

Recently, Yang *et al* [30] have performed a novel series of experiments on thin-film PDATS crystals. Here, a sample with an inter-electrode spacing of 240 μm has a dielectric mask of width 120 μm placed on the sample surface, between the electrodes. Following illumination by a laser pulse of photon energy 3.68 eV, a double-peak photocurrent is observed, with the time interval between the peaks taken as the average time that the charge carrier takes to drift from the middle of the first gap to the middle of the second gap. Based on this interpretation then, they find field saturation of drift velocity for fields between 8×10^5 and 1.5×10^6 V m^{-1}, with the drift velocity deduced to be 50000 m s^{-1}. In addition, with the mask removed, they tightly focus a laser spot on the sample, and observe featureless photocurrents with a peak that shifts in time as the laser spot is moved across the sample. A drift velocity is deduced by shifting the laser spot by a known displacement, and then dividing this by the shift in time of the corresponding peak currents. A drift velocity of 60000 m s^{-1} is found.

We find difficulty, however, in reconciling their results with ours. In their latter experiment which in principal is similar to ours (they localize carrier generation by focusing, we do it by use of a slit), we would expect to find a clearly defined time-of-flight signal with a shoulder and tail, which they do not. A reason for this may be the following and could have some bearing on their double-gap experiment. A conservative estimate for their laser intensity is about 1×10^{10} W m^{-2}. For our experiments, the intensity is about 1×10^5 W m^{-2}. Assuming that in both cases, the quantum efficiency for carrier generation is the same (Yang *et al* and ourselves use similar laser photon energies) and also that the sample capacitances are similar (our inter-electrode spacings are of the same order as theirs), it seems likely, in our view, based on the conclusions of section 3.1, that their experiments are conducted under severe space charge conditions which could result, therefore, in the featureless current decays observed. In our opinion, this leads to some doubt as to the validity of the interpretation by Yang *et al* of their photocurrents. It would be interesting to see, however, whether their results would agree with ours were they to use much lower laser intensities, for the same applied fields.

We now return to the sweep-out experiments of Heeger *et al*. Using equation (12) they are able to plot the field dependence of the carrier drift velocity. This we show in figure 14 along with our own data from figure 10 for comparison. Clearly, our results are in good agreement with theirs.

At this point though, it should be said that Donovan and Wilson have questioned the validity of the experimental arrangement used by Heeger *et al* for determining charge transport in PDATS. Because these objections have some bearing on our own experimental set-up, we state them and then relate them to our own observations.

Donovan and Wilson argue against the use of narrow-gap surface geometry when using highly one-dimensional materials. They maintain that the tail decays observed

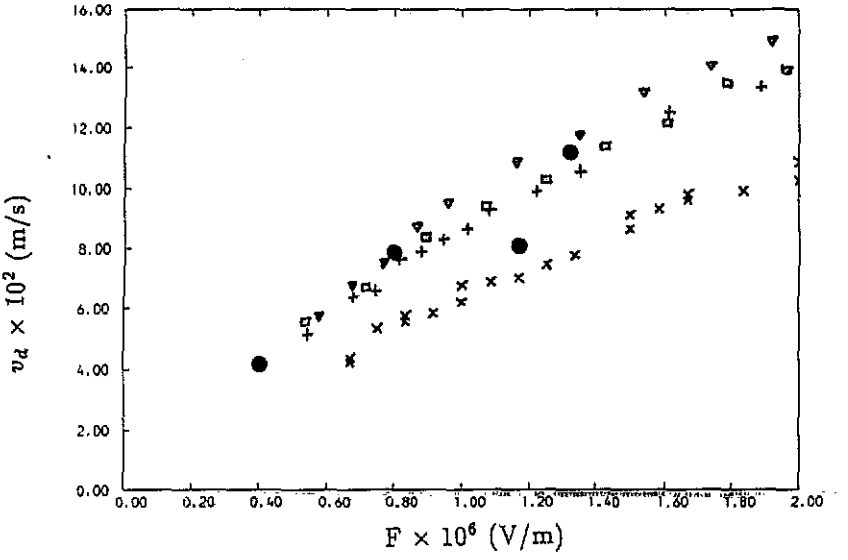

Figure 14. Data from [26] (filled circles) plotted onto data from figure 10.

using samples with such gap sizes are not due to trapping events, but are in fact due to carriers traversing for millimetre distances under the electrodes because they are constrained to drift along the polymer chains [31]. In our experiments though, we see no evidence for this; from inspection of the transit profiles of figure 9, not only does the transit time scale with L, implying that the faster carriers discharge at the edge of the absorbing electrode, but also the tail following the transition region is length dependent, i.e. the tail gets longer as L gets larger. This is because carriers are sampling more traps as they traverse a greater distance leading, therefore, to the slightly more dispersive transit profiles. Hence, the dependence of the tail width with L implies that the slower carriers are also traversing the electrode gap and then discharging, rather than travelling under the electrodes.

Donovan and Wilson also claim that the changes in current profiles observed by Heeger *et al*, when the field is increased, are not due to changes in carrier drift velocity, but are a result of faster bimolecular recombination rates leading to narrower tail decays because of increased carrier concentrations [32, 33]. This argument could also be applied to our observations; as mentioned in section 3.4, using the slit and a positive voltage polarity, we observe a phenomenon similar to that seen by Heeger *et al* and ascribe this to a form of sweep-out. In our experiments though (the results are shown in figure 13), we have kept the current heights the same for both the high and the low field by varying the laser intensity. Since the current height is a convolution of carrier number and carrier velocity, using the same current heights implies that the carrier densities are either the same for both fields (if the drift velocity after 10 ns is the intrinsic-field-saturated SWAP velocity as asserted by Donovan and Wilson) or for the higher field, the carrier density is less than for the lower field (if the drift velocity is a field-dependent trap-limited one as suggested by the transit and sweep-out experiments). In either case then, if bimolecular recombination were present, the lowering of the applied field would result in a narrowing of the current profile. However, we see the reverse effect as the field is lowered and can thus only conclude

that the profile changes we observe are due to the carrier velocity being trap limited.

Finally, we consider the time-of-flight signals observed by Reimer and Bassler, mentioned in section 2. They deduced a mobility of 5×10^{-4} m^2 V^{-1} s^{-1} which is in good agreement with our own observations. However, at that time, they ascribed the transit signals as being due to a free-carrier drift in response to the applied field. These authors are now of the opinion that the observed transits were indeed defect limited [29].

5. Conclusions

In summary, we have demonstrated unambiguous trap-limited transits for the negative carriers with a mobility in good agreement with the work of Bassler *et al* and Heeger *et al*. Inter-trap separations have been shown to be 15 μm or less.

A simple model is proposed that is based on free-chain motion and shallow trapping. This model gives reasonable agreement with the field dependence of drift velocity data and is also compatible with the Gaussian propagation observed.

The absence of time-of-flight signals for the positive carriers at all applied fields used demonstrates a much smaller mobility than that of the negative carriers.

Finally, we have shown that space charge effects need to be considered in order for clearly defined time-of-flight signals to be observed. As such, care is taken to use low laser intensities which thus lead to low carrier densities, for a given field.

So far, these experiments have only been confined to the tens of nanosecond timescales. It would be interesting, therefore, to extend these techniques to the picosecond regime. Then, a better estimation of the inter-trap separation (and direct observation of the on-chain motion) may be possible.

Acknowledgments

We thank Professor D N Batchelder (Leeds University (UK)) for many useful discussions during the course of this work. We are also grateful to Dr B J E Smith for supplying us with some excellent quality PDATS crystals. The experiments presented here were conducted at Queen Mary and Westfield College, London. This work was supported by the SERC (UK).

References

[1] Wegner G 1969 *Z. Naturf.* B **24** 824
[2] Pope M and Swenberg C E 1982 *Electronic Processes in Organic Crystals (Monographs on Physics and Chemistry of Materials 39)* (Oxford: Oxford Science Publications)
[3] Siddiqui A S and Wilson E G 1979 *J. Phys. C: Solid State Phys.* **12** 4237
[4] Poole N J, Smith B J, Batchelder D N and Read R J 1986 *J. Mater. Sci.* **21** 507
[5] Stevens G C, Ando D J, Bloor D and Ghotra J S 1976 *Polymer* **17** 623
[6] Kepler R G 1960 *Phys. Rev.* **119** 1226
[7] LeBlanc Jr O H 1960 *J. Chem. Phys.* **33** 626
[8] Karl N, Schmid E and Seeger M 1969 *Z. Naturf.* A **25** 382
[9] Scharfe M E 1970 *Phys. Rev.* B **2** 5025
[10] Scher H and Montroll E W 1975 *Phys. Rev.* B **12** 2455
[11] Pfister G and Scher H 1978 *Adv. Phys.* **27** 747

[12] Movaghar B, Murray D W, Donovan K J and Wilson E G 1984 *J. Phys. C: Solid State Phys.* **17** 1247
[13] Reimer B and Bassler H 1978 *Phys. Status Solidi* b **85** 145
[14] Donovan K J, Fisher N E and Wilson E G 1989 *Synth. Met.* **28** D557
[15] Donovan K J and Wilson E G 1981 *Phil. Mag.* B **44** 9
[16] Lochner K, Reimer B and Bassler H 1976 *Phys. Status Solidi* b **76** 533
[17] Fisher N E 1990 *PhD Thesis* University of London
[18] Many A, Weisz S Z and Simhony M 1962 *Phys. Rev.* **126** 1989
[19] Many A and Rakavy G 1962 *Phys. Rev.* **126** 1980
[20] Schwartz L M and Hornig J E 1965 *J. Phys. Chem. Solids* **26** 1821
[21] Leyrer R J, Wegner G and Wettling W 1978 *J. Phys. Chem.* **82** 697
[22] Wilson E G 1983 *J. Phys. C: Solid State Phys.* **16** 6739
[23] Wilson E G 1979 *J. Phys. C: Solid State Phys.* **13** 2885
[24] Marshall J M 1977 *Phil. Mag.* **36** 959
[25] Moses D, Sinclair M and Heeger A J 1987 *Phys. Rev. Lett.* **58** 2710
[26] Moses D and Heeger A J 1989 *J. Phys. C: Solid State Phys.* **1** 7395
[27] Donovan K J, Freeman P D and Wilson E G 1985 *Electronic Properties of Polymers and Related Compounds (Springer Series in Solid State Sciences 63)* (Berlin: Springer) pp 256–62; 1985 *Proc. IWEPP (Austria)*
[28] Donovan K J and Wilson E G 1985 *J. Phys. C: Solid State Phys.* **18** L51
[29] Blum T and Bassler H 1988 *J. Chem. Phys.* **123** 431
[30] Yang Y, Lee J Y, Miller P, Li L, Kumar J and Tripathy S K 1991 *Solid State Commun.* **77** 763
[31] Donovan K J and Wilson E G 1989 *Synth. Met.* **28** D563
[32] Donovan K J and Wilson E G 1990 *J. Phys. C: Solid State Phys.* **2** 1659
[33] Donovan K J, Elkins J W P and Wilson E G 1991 *J. Phys. C: Solid State Phys.* **3** 2075